Room temperature ferromagnetic resonance in hetero-epitaxial BTO - BFO/LSMO magnetoelectric composite

Benjamin Madon, Han Byul Kang, Min Gyu Kang, Deepam Maurya, Brenden A. Magill, Marcos J. P. Alves, Jean-Eric Wegrowe, Henri-Jean Drouhin, Shashank Priya, and Giti A. Khodaparast

Room temperature ferromagnetic resonance in hetero-epitaxial *BTO − BFO/LSMO* magnetoelectric composite

Benjamin Madon,[1,a] Han Byul Kang,[2,a] Min Gyu Kang,[2] Deepam Maurya,[2] Brenden A. Magill,[3] Marcos J. P. Alves,[1] Jean-Eric Wegrowe,[1] Henri-Jean Drouhin,[1] Shashank Priya,[2] and Giti A. Khodaparast[3,b]

[1]*Laboratoire des Solides Irradiés, CNRS UMR 7642, CEA-DSM-IRAMIS, École Polytechnique, Université Paris-Saclay, 91128 Palaiseau cedex, France*
[2]*Center for Energy Harvesting Materials and Systems (CEHMS), Bio-Inspired Materials and Devices Laboratory (BMDL), Virginia Tech, Blacksburg, Virginia 24061, USA*
[3]*Department of Physics, Virginia Tech, Blacksburg, Virginia 24061, USA*

We synthesized epitaxial BTO-BFO heterostructure with decreased leakage and simultaneously improved the multiferroic properties. This study provides new direction for ferromagnetic resonance studies, in high quality BTO-BFO films grown on LSMO. We observed small Gilbert damping (α=0.004) and the absence of large inhomogeneous broadening, in a film with 80 nm thickness of BTO-BFO on LSMO (110). This fact offers opportunities for employing this material system for spin transfer in multifunctional materials where controlling magnetization by a flow of spin angular momentum, or spin current, is crucial toward developing nanoscale spin-based memory and devices. Magnetic insulators, such as BTO-BFO on LSMO, are potentially excellent candidates for pure spin current without the existence of charge current. © *2018 Author(s). All article content, except where otherwise noted, is licensed under a Creative Commons Attribution (CC BY) license (http://creativecommons.org/licenses/by/4.0/).* https://doi.org/10.1063/1.5037165

INTRODUCTION

Multiferroics are highly promising for development of multifunctional devices, that utilize coupling between optical, electrical, and magnetic degrees of freedom,[1–7] such as ultra-fast non-volatile ferroelectric memory,[3,8] spintronic devices[4] and energy harvesters.[9,10] However, developing single-phase multiferroics with high magnetoelectric coupling coefficient, has been a challenge. Ferroelectricity requires empty d-orbitals for cation off-center displacement, while ferromagnetism arises from partially filled d-orbitals.[11] This contrary requirement presents challenge in designing material compositions, with room temperature multiferroic property. In a multiferroic composition the ions that constitute the electric dipole moment by being off-centered and those that induce magnetic moments, should be contributed from disparate sources. For example, multiferroicity of bismuth ferrite (BFO), which is one of the most studied multiferroics[1–4,6,8–10] arises from two contributions of stereochemical activity, the ion pair on large (A-site) cation contributes to ferroelectricity and the small magnetic transition metal (B-site) cation provides magnetism.[12] BFO is a promising single-component multiferroic with high Curie temperature $T_c = 1103$ K but it suffers from leaky ferroelectric behavior, mainly due to the volatilization of Bi, resulting in the valence fluctuation of Fe ions from Fe^{3+} to Fe^{2+} and formation of oxygen vacancies. In our prior study, we reported a single-phase $(1 − x)BaTiO_3 − xBiFeO_3$ (BTO-BFO) materials with high room-temperature magnetoelectric (ME) voltage coefficient (0.87 *mV/cmOe*) and high piezoelectric properties ($g_{33} = 18.5 \times 10$ *mV mN^{-1}*

---

[a]Authors with equal contributions.

[b]Corresponding author: khoda@vt.edu

and $d_{33} = 124 \ pCN^{-1}$), due to local monoclinic distortions within rhombohedral phase at a specific composition of $x = 0.725$.[5]

In this study, we probe ferromagnetic resonance (FMR) in solid solutions of BTO-BFO grown on $La_{0.67}Sr_{0.33}MnO_3$ (LSMO). FMR is one of the basic methods for probing the magnetic states, when the system is excited out of the equilibrium, resulting in a uniform motion of the magnetization, known as spin waves. Dissipation in ferromagnetic systems after the excitation out of equilibrium, is of fundamental interest for understanding the magnetization dynamics. For example, probing and controlling magnetic damping, could be important for reducing the switching current and increasing the speed in magnetic memory devices, triggered by spin-torque. In magnetic materials, damping of magnetization precession due to the energy transfer from the spin system to the lattice, can be parameterized as a scalar, α, known as the Gilbert damping parameter. Within the Landau-Lifschitz-Gilbert (LLG) frame of magnetization dynamics,[13] we can write:

$$\frac{\partial M}{\partial t} = -\gamma M \times H_{eff} + \alpha M \times \partial M / \partial t + \tau \tag{1}$$

where M is the magnetization unit vector, γ is the gyromagnetic ratio, H_{eff} is an effective magnetic field determined by the external applied magnetic field in addition to the exchange stiffness, dipole field, and anisotropy field due to presence of the spin-orbit interactions. In Eq. (1), α is the Gilbert damping constant and τ represents the current-induced torques. Figure 1 presents the magnetization dynamics described by Eq. (1). The second term on the right side of Eq. (1) defines the relaxation of the magnetization towards the effective field, while the first term leads to precession of the magnetization about the effective magnetic field, and τ is the current-induced torque.

For developing spintronic devices, magnetic materials systems with a low Gilbert damping parameter α are desirable, in order to achieve excitation and propagation of spin dynamics with low energy input.[14] Insulating magnetic materials could demonstrate lower damping coefficients compared to hetero-epitaxial films of magnetic metals, where the spin dissipation processes from conduction electron scattering[15,16] doesn't exist. Thin-film magnetic insulator yttrium iron garnet (YIG) has shown sufficiently low damping on the order of 10^{-4}.[17] Other than YIG, there are only limited studies quantifying the Gilbert damping parameter of thin-film magnetic insulators.[18,19] This indicates the challenges in conducting studies on insulating thin-film materials where microwave FMR techniques are required. Recently, magnetically soft epitaxial spinel NiZnAl-ferrite thin films, with low Gilbert damping parameter ($\alpha \sim 3 \times 10^{-3}$), have been reported.[18] Here we provide new understanding of FMR in high quality BTO-BFO films grown on LSMO which provides promising heterostructure platform.
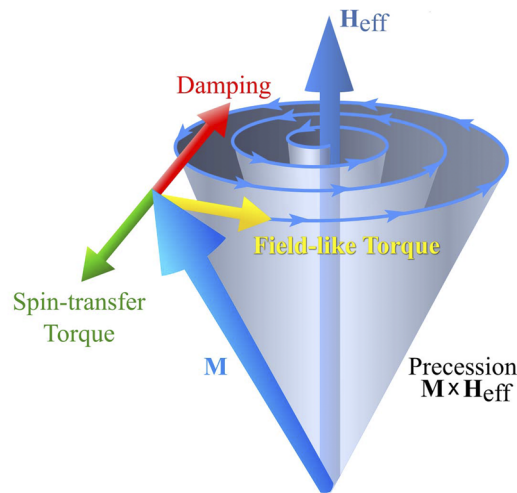
FIG. 1. The magnetization M precesses about the effective field direction (H_{eff}). The damping torque moves the magnetization toward the effective field direction. Spin-transfer torque and field-like torque are shown by green and yellow arrows, respectively.

Composites of layered ferromagnetic (FM) materials and anti-ferromagnetic (AFM) materials or ferroelectric (FE) materials display a multitude of interface interactions that can alter the hysteresis loop of the FM layer. These effects include: exchange bias coupling on the interface between FM and AFM materials,[20,21] strain mediated magnetoelectric (ME) coupling,[22,23] spin-polarized charge mediated ME coupling,[24,25] and voltage controlled ME coupling.[26,27] Multiferroic materials allow the possibility of creating layered devices that exploit one or more of these interface effects. In this study, we observed the enhancement of the effective saturation magnetization (<*Ms*>) in epitaxial films of LSMO capped with BTO-BFO films, through FMR measurements. A similar enhancement was observed in LSMO capped with BFO and could be related to an interface effect and spin-orbit couplings.[28]

MATERIALS CHARACTERISTICS

As shown in Fig. 2a, we synthesized novel hetero-epitaxial composites composing of multiferroic BTO-BFO and ferromagnetic LSMO with varying layer thickness ratios. Hetero-epitaxial BTO-BFO/LSMO thin films were grown on (001), and (110) oriented $SrTiO_3$ (STO) substrates by off-axis RF magnetron sputtering. Prior to film deposition, the surface of the STO substrates was treated by buffered oxide etchant (BOE) and subsequently annealed at 900° C under an O_2 atmosphere to make Ti-terminated surface. The LSMO thin film was deposited at 600^oC under 5 mTorr of pressure with O_2:Ar ratio of 8:2 and RF power of 4.93 W/cm^2. BTO-BFO thin film was grown on the epitaxial LSMO layer at 400 ^oC using an in-situ deposition under the same RF power and pressure O_2:Ar gas ratio of 1:9. Next, we studied the crystallographic orientation dependence of magnetic properties in LSMO thin films. Larger magnetic moment and higher *Tc* was observed in (110)-oriented LSMO films compared to (001)-oriented LSMO films. This observation is taking into account, the difference of ABO$_3$ perovskite stacks, on crystallographic orientations of substrates. In ABO$_3$ perovskite system, was observed in (110)-oriented ABO$_3$ is composed of alternating $[ABO]^{4+}$ and O_2^{4-} planes, while (001)-oriented perovskite comprises of alternating $[AO]^{0.7^+}$ and $[BO_2]^{0.7^-}$ layers.[29,30]
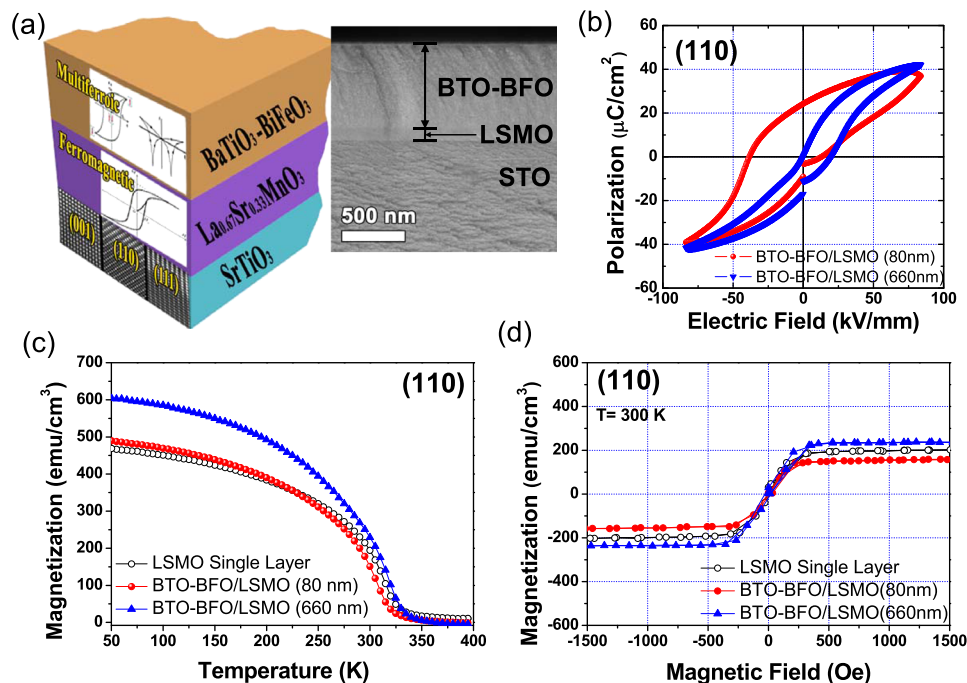
FIG. 2. (a) Schematic illustration and TEM image of BTO-BFO/LSMO heterostructure. (b) P-E curve of BTBFO/LSMO hetero-epitaxial films, (c) Temperature dependence of magnetization in the composite films (d) Room temperature magnetization of the films as a function of magnetic field.

TABLE I. Materials characteristics and magnetic properties of four samples studied in this work including thickness, film orientation, (T_c), saturated magnetization (M_{sat}) **from SQUID measurements**, remanent magnetization (M_r), coercive field (H_c), and Gilbert damping (α). All films were grown on STO substrates. Sample 3 and 4 were grown on sample 2.

Sample	Thickness (nm)	T_c K	Growth Direction	Structure	M_{sat} (emu/cm^3)	M_r (emu/cm^3)	Hc^- (Oe)	Hc^+ (Oe)	Damping (α)
1	100	285	(100)	LSMO	31.896	5.31	-98.04	100.65	0.08
2	100	327	(110)	LSMO	200.69	30.42	-23.14	-2.14	0.011
3	660	333.48	(110)	BTO-BFO/LSMO	235.17	4.74	-6.63	7.054	-
4	80	323.08	(110)	BTO-BFO/LSMO	157.93	30.03	-12.72	3.87	0.004

The coherent polar surface in (110) orientation may be more susceptible to reconstruction and strain relaxation, resulting in faster recovery of spin moment as a function of film thickness compared to (001) surface.[29,31] As a result, (110)-oriented LSMO film showed 5 times larger magnetization at room temperature compared to (001)-oriented LSMO film. Therefore, we focused on the (110)-oriented LSMO films to investigate the novel hetero-epitaxial BTO-BFO/LSMO composites.

Figure 2b shows ferroelectric loops of (110)-oriented BTO-BFO/LSMO films as a function of the film thickness. The saturated polarization was similar between thin (80nm) and thick (660 nm) BTO-BFO films, however, coercive field and loop shape were changed with increasing film thickness. The thicker BTO-BFO film had a higher polycrystallinity, and thus, having more defects and pinning centers that introduces lower coercive field and lossy shaped loops. Figure 2c shows the temperature dependence of magnetization, and Fig. 2d represents the room temperature magnetization of the thin and thick BTO-BFO/LSMO films as well as just LSMO film. Thin BTO-BFO/LSMO film shows slightly smaller magnetization at low temperature compared to thicker BTO-BFO/LSMO film. By depositing BTO-BFO layer to LSMO film, the near surface layer on LSMO film experiences tensile strain due to lattice misfit with BTO-BFO (3.984 Å).

However, in this case, the variation of magnetic properties in the BTO-BFO/LSMO heterostructure is not directly correlated with the tensile strain changes in the films, due to the non-strain mediated magnetic coupling between the BFO and the LSMO layers at the interface. Yu *et al.* reported that new magnetic phase can be generated in thin films due to electronic orbital reconstruction between the Mn and Fe orbitals, providing novel magnetic state localized at the interface.[32] Rao *et al.* have also demonstrated the enhancement in magnetic moment and improved magnetic hysteresis squareness resulting from complex interplay between orbital and spin degree of freedom in BFO/LSMO heterostructure grown on Si.[28] Therefore, we can consider that the misfit strain in the film and the interaction of electronic orbital between Mn and Fe ions at the interface simultaneously contributes to the variation of magnetic properties in the bilayer structure.

For a deeper understanding of the ferromagnetism in BTO-BFO/LSMO heterostructure, we performed FMR characterization at room temperature on 4 samples described in Table I. Our results provide key information on the ferromagnetic nature of these unique material systems.

FERROMAGNETIC RESONANCE IN BTO-BFO/LSMO

The basic procedure for FMR characterization is presented in the supplementary material where we also present the FMR measurements of 100 nm thick LSMO films. This thickness was an optimum layer thickness for LSMO to observe FMR in this materials system at RT. The exact same LSMO (110) film, described in the supplementary material (sample 2, **presented in supplementary material**), was used for growing BTO-BFO epitaxial layer, and the TEM image of the heterostructure is shown in Fig. 2a. The FE loops in Fig. 2b represent the high quality FE property, and the SQUID measurements shown in Fig. 2c demonstrates good ferromagnetic property. In BTO-BFO heterostructures, the stacking of the two perovskites decreases the overall conductivity of the material and simultaneously improves the multiferroic properties of the system.[6]

Fig. 3a shows the observed FMR for the sample 3 (660 nm BTO-BFO/LSMO (110) film), from 1 GHz to 3 GHz. At 1 GHz the peak looks symmetric and it is in fact a mixture of two asymmetric
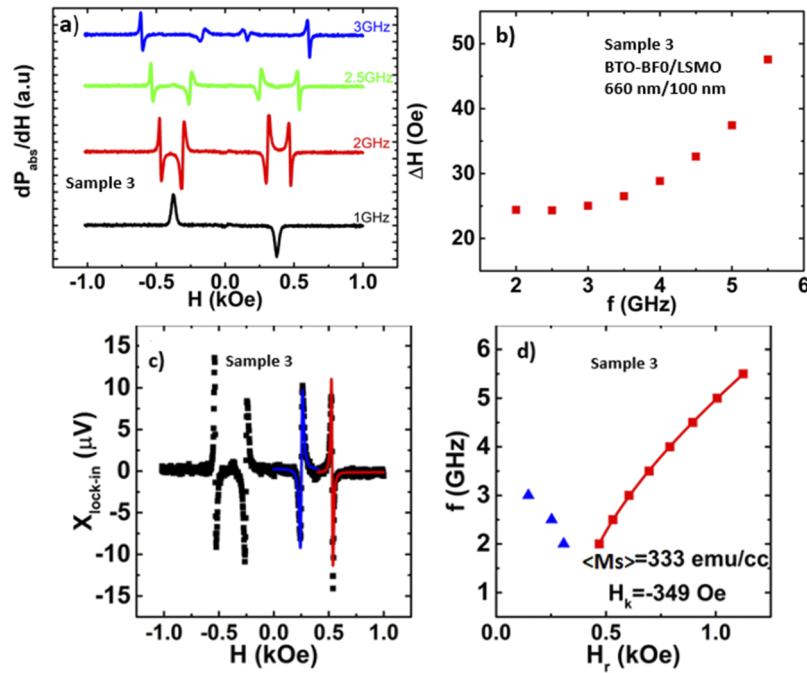
FIG. 3. (a) Derivative of the absorbed power as a function of the applied magnetic field for different RF resonance frequencies ranging from 1-3 GHz. (b) The observed non-linear ΔH in this sample does not allow to extract the damping in the available frequency and magnetic field ranges. (c) Focusing only on one of the resonances. Black-dots are the experimental data corresponding to the derivative of the absorbed power at 2 GHz. The anti-Lorenzian fits to the low- and high field resonances are shown by the blue and red curves, respectively. (d) Resonance frequency as a function of the resonance field. Triangular blue symbols are representing the resonance frequencies at the low fields and the red square ones are the resonance frequencies at the high field peak. The red line is a fit to Kittel's formula for the high field peak. $<M_s>$ of 333 emu/cc, noted on the graph is referring to the extracted saturation magnetization from the FMR measurements.

Lorentzian line shapes. With increasing frequency, we observed two resonances, both of which could be fitted to anti-Lorentzian line shape. Surprisingly, the low frequency peak, where the ferromagnetic anti-resonance peaks are related to non-saturated states,[33] moves toward low fields by increasing the frequency until it vanishes, and at the same time the amplitude of the high frequency resonance increases with increasing frequency. In addition, the linewidth ΔH, of the high field resonance frequency peaks were extracted. Figure 3b shows the linewidth as a function of frequency for the high frequency resonances of the 660 nm BTO-BFO/LSMO (110) film.

Focusing only on one of the resonances, Fig. 3c, presents an example of the FMR at 2 GHz for sample 3. We fitted each peak with an anti-Lorentzian profile and extracted the resonance field for both peaks. Figure 3d) shows the frequency as a function of the resonant field (H_r), where blue triangles are for the low frequency resonance and the red squares, indicate the high field frequency peaks. We extracted $<M_s>$ (the effective magnetization per unit volume) of 333 emu/cm³ and $H_k = -349$ Oe, by fitting to the high field frequency resonance using Eq. (2). In this case, $<M_s>$ is slightly higher than that of the saturation magnetization from SQUID, presented in Fig. 2d, but lower than the extracted $<M_s> = 814 emu/cm^3$ value for LSMO (110), presented in the supplementary materials. For this sample, no damping could be extracted, using Eq. (3), as the observed trend is not linear, in the available frequency and magnetic field ranges. This non-linearity could originate from two-magnon scattering[34] which is a non-Gilbert damping.[35,36]

$$f = (\gamma/2\pi)\sqrt{(H_r + H_k)(H_r + H_k + 4\pi <M_s >)} \qquad (2)$$

In a Gilbert damping regime, the damping coefficient, α can be extracted from the frequency dependence of ΔH according to:

$$\Delta H = \frac{4\pi\alpha f}{\gamma} + \Delta H_0 \tag{3}$$

In general, the Gilbert Damping is dominated by direct relaxation to the lattice, when the system is out of the thermodynamic equilibrium. It is well-known that a second relaxation process is possible in the presence of a FMR structural inhomogeneity, which can generate magnons scattering within the magnetic subsystem.[34] Therefore, the uniform motion of the magnetization during precession or flips, in a given magnetic system may populate excited states. As reported earlier, FMR measurements on various magnetic nanostructures demonstrated nonlinear linewidth (ΔH) dependence on frequency. This fact was attributed to the superposition of two relaxation processes, the Gilbert damping, and the scattering of spin wave excitations within the magnetic subsystem (such as magnon-magnon scattering).[34] Two-magnon scattering processes can occur due to the defects or inhomogeneities in the crystal structure.[37]

As shown in Fig. 4a, we observed FMR in a BTO-BFO film with 80 nm thickness (sample 4) at RT, from 2.5-9 GHz, where only single resonance peak is observed. This could be related to lower structural disorder and can explain low damping. In this case, both the effective saturated magnetization $<M_s>$ of 750 emu/cm^3 and damping (α) of 0.004 were extracted, using the data presented in Fig. 4b and Fig. 4c, respectively. The observed small Gilbert damping in this structure is a promising observation close to reported value of epitaxial NiZnAl-ferrite.[18]

In this film the saturation magnetization, measured by SQUID at ~ 300 K (M_{sat}), presented in Fig. 4d, is by a factor of 5 smaller compared to the measured FMR effective saturation magnetization ($<M_s>$), in Fig. 4c. This fact could indicate the presence of a large uniaxial anisotropy field.[18] In addition, unlike the 660 nm thick film, the $<M_s>$ for the 80 nm film did not change significantly compared to the $<M_s>$ of LSMO (110).
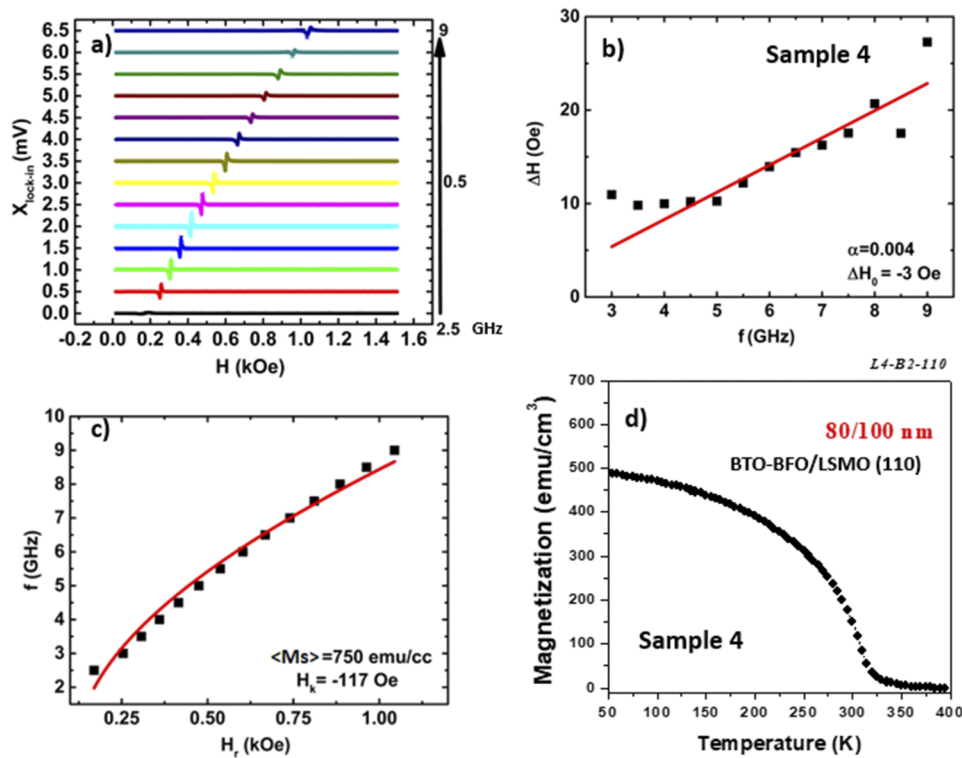
FIG. 4. (a) FMR response of Sample 4. (b) Resonance frequency as a function of the resonant field. b) Linewidth as a function of the RF frequency. The red line is a linear fit from which the damping parameter α = 0.004 is extracted using Eq. (3). (c) Frequency as a function of the magnetic field at resonance. The red curve is the best fit obtained from Kittel formula. $<M_s>$ of 750 emu/cc, noted on the graph is referring to the extracted saturation magnetization from the FMR measurements. (d) Magnetization as a function of temperature obtained from SQUID.

CONCLUSION

We synthesized epitaxial BTO-BFO, heterostructure with decreased leakage and simultaneously improved the multiferroic properties. While only limited thin-film magnetic insulators with low Gilbert damping parameter exist,[18,19] this study provides new direction for FMR studies, in high quality BTO-BFO films grown on 100 nm LSMO (110). We have identified optimum LSMO and BTO-BFO thicknesses to observe FMR at RT. This heterostructures can be important for spin transfer in multifunctional materials where controlling magnetization by a flow of spin angular momentum, or spin current. Magnetic insulators are potentially excellent candidates for pure spin current without the existence of charge current. In this scheme, the spin accumulation will interact with the magnetic moments of the insulator layer, resulting in spin torques which can initiate precession and switching without the spin-polarized electrons entering the insulator layer is crucial toward developing nanoscale spin-based memory and devices.[38–40] The observed small Gilbert damping after growing 80 nm of BTO-BFO on LSMO (110) and the absence of large inhomogeneous broadening offer opportunities for employing this material system for multifunctional[41–45] devices with lower energy consumption compared to the conventional metallic counterparts. The small reduction of $<Ms>$ in 80 nm thick film (sample 4) compared to the LSMO (110) (sample 2), as well as the expected lower structural disorder in the thinner structure compared to sample 3, could be important when it comes to further development of these material systems for FMR studies.

SUPPLEMENTARY MATERIAL

See the supplementary material for the experimental set up and the FMR measurements on the LSMO films, summarized in Table I.

ACKNOWLEDGMENTS

[1] W. Eerenstein, N. D. Mathur, and J. F. Scott, Nature **442**, 759 (2006).

[2] C.-W. Nan, M. I. Bichurin, S. Dong, D. Viehland, and G. Srinivasan, J. Appl. Phys. **103**, 031101 (2008).

[3] M. Bibes and A. Barthélémy, Nature Materials **7**, 425 (2008).

[4] S. Fusil, V. Garcia, A. Barthélémy, and M. Bibes, Annu. Rev. Mater. Res. **44**, 91 (2014).

[5] S.-C. Yang, V. Kumar, V. Petkov, and S. Priya, Journal of Applied Physics **113**, 144101 (2013).

[6] X. Yang, Z. Zhou, T. Nan, Y. Gao, G. M. Yang, M. Liu, and N. X. Sun, J. Mater. Chem. C **4**, 234 (2016).

[7] T.-J. Park, G. C. Papaefthymiou, A. J. Viescas, Y. Lee, H. Zhou, and S. S. Wong, Phy. Rev. B **82**, 024431 (2010).

[8] D. S. Rana, I. Kawayama, K. Mavani, K. Takahashi, H. Murakami, and M. Tonouchi, Adv. Mater. **21**, 2881 (2009).

[9] J. Seidel, D. Fu, S.-Y. Yang, E. Alarn-Llad, J. Wu, R. Ramesh, and J. W. Ager, Phys. Rev. Lett. **107**, 126805 (2011).

[10] D. Cao, C. Wang, F. Zheng, W. Dong, L. Fang, and M. Shen, Nano Lett. **12**(6), 2803 (2012).

[11] N. A. Spaldin and M. Fiebig, Science **309**(5733), 391 (2005).

[12] R. Ramesh and N. A. Spaldin, Nature Materials **6**(1), 21 (2007).

[13] S. Lepadatu, A. Vanhaverbeke, D. Atkinson, R. Allenspach, and C. H. Marrows, Phys. Rev. Lett. **102**, 127203 (2009).

[14] M. J. P. Alves, D. E. Gonzalez-Chavez, F. Bohn, and R. L. Sommer, Journal of Applied Physics **117**, 123913 (2015).

[15] B. Heinrich, "Spin relaxation in magnetic metallic layers and multilayers," in *Ultrathin Magnetic Structures III*, J. A. C. Bland and B. Heinrich, eds. (Springer-Verlag, 2005), pp. 143–210.

[16] C. K. A. Mewes and T. Mewes, "Relaxation in magnetic materials for spintronics," in *Handbook of Nanomagnetism: Applications and Tools* (Pan Stanford, 2015), pp. 71–95.

[17] H. Chang, P. Li, W. Zhang, T. Liu, A. Hoffmann, L. Deng, and M. Wu, IEEE Magn. Lett. **5**, 6700104 (2014).

[18] S. Emori, B. A. Gray, H.-M. Jeon, J. Peoples, M. Schmitt, K. Mahalingam, M. Hill, M. E. McConney, M. T. Gray, U. S. Alaan, A. C. Bornstein, P. Shafer, A. T. N'Diaye, E. Arenholz, G. Haugstad, K.-Y. Meng, F. Yang, D. Li, S. Mahat, D. G. Cahill, P. Dhagat, A. Jander, N. X. Sun, Y. Suzuki, and B. M. Howe, Adv. Mater. **29**, 1701130 (2017).

[19] A. V. Singh, B. Khodadadi, J. B. Mohammadi, S. Keshavarz, T. Mewes, D. S. Negi, R. Datta, Z. Galazka, R. Uecker, and A. Gupta, Adv. Mater. **29**(30), 1701222 (2017).

[20] W. H. Miekeljohn and C. P. Bean, Phys. Rev. Lett. **102**, 1413 (1956).

[21] S. M. Wu, S. A. Cybart, D. Yi, J. M. Parker, R. Ramesh, and R. C. Dynes, Phys. Rev. Lett. **110**, 067202 (2013).

[22] P. Zhao, Z. Zhao, D. Hunter, R. Suchoski, C. Gao, S. Mathews, M. Wuttig, and I. Takeuchi, Appl. Phys. Lett. **94**, 243507 (2009).

[23] H. Greve, E. Woltermann, H.-J. Quenzer, B. Wagner, and E. Quandt, Appl. Phys. Lett. **96**, 182501 (2010).

[24] C.-G. Duan, J. P. Velev, R. F. Sabirianov, W. N. Mei, S. S. Jaswal, and E. Y. Tsymbal, Appl. Phys. Lett. **92**, 122905 (2008).

[25] H. Y. Guo, J. G. Lin, J. C. Yang, and Y. H. Chu, Appl. Phys. Lett. **105**, 112406 (2014).

[26] H. Ohno, D. Chiba, F. Matsukura, T. Omiya, E. Abe, T. Dietl, Y. Ohno, and K. Ohtani, Nature **408**, 944 (2000).

[27] D. Chiba, M. Sawicki, Y. Nishitani, Y. Nakatani, F. Matsukura, and H. Ohno, Nature **455**, 515 (2008).

[28] S. S. Rao, J. T. Prater, F. Wu, C. T. Shelton, J.-P. Maria, and J. Narayan, Nano Lett. **13**(12), 5814 (2013).

[29] A. I. Volokitin and B. N. J. Persson, Physical Review B **83**(6), 241407(R) (2011).

[30] A. Pojani, F. Finocchi, and C. Noguera, Surface Science **442**(2), 179 (1999).

[31] S. Majumdar and S. van Dijken, Journal of Physics D: Applied Physics **47**(3), 034010 (2013).

[32] P. Yu, J.-S. Lee, S. Okamoto, M. D. Rossell, M. Huijben, C.-H. Yang, Q. He, J. X. Zhang, S. Y. Yang, M. J. Lee, Q. M. Ramasse, R. Erni, Y.-H. Chu, D. A. Arena, C.-C. Kao, L. W. Martin, and R. Ramesh, Physical Review Letters **105**(2), 027201 (2010).

[33] F. J. Rachford and C. Vittoria, Journal of Applied Physics **52**, 2253 (1981).

[34] K. Lenz, H. Wende, W. Kuch, and K. Baberschke, Phys. Rev. B **73**, 144424 (2006).

[35] H. K. Lee, I. Barsukov, A. G. Swartz, B. Kim, L. Yang, H. Y. Hwang, and I. N. Krivorotov, AIP Adv. **6**, 055212 (2016).

[36] S. Emori, U. S. Alaan, M. T. Gray, V. Sluka, Y. Chen, A. D. Kent, and Y. Suzuki, Phys. Rev. B **94**, 224423 (2016).

[37] D. Roy, S. Sakshath, G. Singh, R. Joshi, S. V. Bhat, and P. S. Anil KumaJ, Phys. D: Appl. Phys. **48**, 125004 (2015).

[38] A. Brataas, A. D. Kent, and H. Ohno, Nat. Mater. **11**, 372 (2012).

[39] D. C. Ralph and M. D. Stiles, J. Magn. Magn. Mater. **320**, 1190 (2008).

[40] L. Liu, T. Moriyama, D. C. Ralph, and R. A. Buhrman, Phys. Rev. Lett. **106**, 036601 (2011).

[41] B. A. Magill, K.-D. Park, Y. Zhou, A. Chopra, D. Maurya, S. Priya, M. Raschke, A. Belyanin, C. J. Stanton, and G. A. Khodaparast, Energy Harvesting and Systems. **3**(3), 229 (2017).

[42] B. A. Magill, M. Bishop, S. A. McGill, Y. Zhou, A. Chopra, H.-C. Song, C. J. Stanton, S. Priya, and G. A. Khodaparast, Proc. of SPIE **9551**, 95510T (2015).

[43] M. A. Meeker, S. Kundub, D. Maury, M.-G. Kang, A. Sosa, R. R. H. H. Mudiyanselage, M. Clavel, S. Gollapudi, M. K. Hudait, S. Priya, and G. A. Khodaparast, Optical Materials **73**, 793 (2017).

[44] M. Ulman, D. W. Bailey, L. H. Acioli, F. G. Valle, C. J. Stanton, E. P. Ippen, and J. G. Fujimoto, Physical Review B **47**, 10267 (2013).

[45] S. Davis, A. Baruth, and S. Adenwalla, Applied Physics Letters **97**, 232507 (2010).